Density Functional Theory of the Cu_A-Like Cu_2S_2 Diamond Core in $Cu^{II}_2(NGuaS)_2Cl_2$

M. Witte,*[a] U. Gerstmann,[a] A. Neuba,[b] G. Henkel,[b] and W. G. Schmidt[a]

Density functional theory (DFT) calculations with localized as well as plane-wave basis functions are performed for the recently reported dicopper thiolate species $Cu_2(NGuaS)_2Cl_2$ [NGuaS = 2-(1,1,3,3-tetramethylguanidino) benzenethiolate, $C_{11}H_{16}N_3S$] and its bromo derivative [Neuba *et al*., Angew. Chem. Int. Ed. 2012, 51, 1714.]. For both hybrid and semilocal functionals, the neutral complexes are found to have broken symmetry (BS) character, with electron paramagnetic resonance silent, antiferromagnetically coupled [$Cu^{2+}...Cu^{2+}$] site in which the coupling is driven by super exchange interaction within the Cu_2S_2 diamond core. The accurate theoretical description of the geometric structure, however, provides a major challenge for DFT: (*i*) the multideterminant character of the ground state wave function has to be covered by the BS approach. It requires (*ii*) metageneralized gradient approximations, that is hybrid functionals with an explicit dependence on the kinetic energy of the individual orbitals: In combination with a dispersion correction, the metafunctional TPSSh results in a Cu—Cu distance close to the experimentally observed value of 2.7 Å. For the negative charge state of the complex, a mixed-valent [$Cu^{1.5+}...Cu^{1.5+}$] electronic structure with a smaller Cu—Cu distance of 2.6 Å is predicted, similar to the value of the Cu_A site of cytochrome *c* oxidase. © 2016 Wiley Periodicals, Inc.

DOI: 10.1002/jcc.24289

Introduction

The dinuclear copper core is essential for metal-based electron transfer in the Cu_A site of cytochrome *c* oxidase, the terminal enzyme of aerobic respiration in eukaryotic organisms, as well as the nitrous oxide reductase found in denitrifying bacteria.[1–7] A wide range of spectroscopic studies including extended X-ray absorption fine structure,[4,5] electron paramagnetic resonance (EPR),[8,9] optical absorption,[10,11] low-temperature magnetic circular dichroism,[12] resonance Raman,[13] and X-ray crystallography[1–3,14] addressed its electronic and structural properties and concluded on a rhombic geometry, that is the "diamond" core, where the two Cu atoms are separated by a short distance of about 2.44 Å. They are bridged by two S(Cys) atoms and coordinated to two N(His) ligands. Electron nuclear double resonance studies on various Cu_A species found an electronic structure of a $S = 1/2$ state.[8,9,15–19] Hence, the singly occupied molecular orbital (SOMO) shows a delocalized character. For the Cu_A site in nitrous oxide reductase, for example, about 90% of the magnetization density is found to be equally distributed over the central Cu and S atoms of the diamond core; a considerable part of the unpaired electron spin density (up to 5%) is also found on the N(His) ligands.[20] Hence, the natural Cu_A complex is an open shell system with an unpaired electron delocalized over the Cu_2S_2 core, resulting in a mixed-valent [$Cu^{1.5+}...Cu^{1.5+}$] state.

Generally, Cu(II) centers can be classified into three types based on their EPR and optical spectroscopical data: "blue" (type-1), "nonblue" (type-2), and "dinuclear" (type-3) species. The blue copper site in plastocyanin, also being thiolate bridged,[21] has been studied in detail,[22–26] and it has been found that the Cu–thiolate bonds, like metal–thiolate bonds, in general, are strongly covalent.[27] It has been shown that type-1 centers can be structurally converted into purple Cu_A centers.[28] The synthesis of dinuclear mixed-valent copper(II) thiolate complexes with active-site properties comparable to those of the natural Cu_A has been a challenge for synthetic inorganic chemistry for some time.[29–40] The first, though not reversibly reducible, mixed-valent complex has been developed by Tolman and coworkers[41] and theoretically characterized by Solomon et al.[42] Duboc and coworkers succeeded in synthesizing a mixed-valent thiolate bridged complex, showing biomimetic functionality.[43] Although the redox reaction is slower than for the natural Cu_A site, it is still faster than for Cu(II) complexes utilizing plastocyanin.[44]

Recently, Neuba et al.[45] reported a previously unknown chloride-induced disulfide-thiolate interconversion, leading to the copper(I) disulfide complex cation $[Cu^{I}_2\{(NGuaS-)_2\}_2]^{2+}$ to the electrically neutral, blue copper(II) thiolate species $[Cu^{II}_2(NGuaS)_2Cl_2]$ (hereafter: **1**) (scheme, Fig. 1)*. Owing to its symmetry, the neutral complex has an even number of electrons and, thus, cannot show Cu_A functionality. Nevertheless, it (i) can be used for analyzing the exchange coupling in the Cu_2S_2 diamond core, (ii) may serve as a structural model for Cu_A centers, and (iii) represents a possible

[a] *M. Witte, U. Gerstmann, W. G. Schmidt*
Department of Physics, Lehrstuhl Für Theoretische Materialphysik, Universität Paderborn Paderborn 33098, Germany
E-mail: mwitte@mail.upb.de
[b] *A. Neuba, G. Henkel*
Department of Chemistry, Lehrstuhl Für Anorganische Chemie, Universität Paderborn, Paderborn 33098, Germany
Contract grant sponsor: Deutsche Forschungsgemeinschaft; Contract grant number: FOR1405; Contract grant sponsor: Höchstleistungs-Rechenzentrum Stuttgart (HLRS)
NGuaS: = o—SC_6H_4N=$C(NMe_2)_2$ (i.e., $C_{11}H_{16}N_3S$)

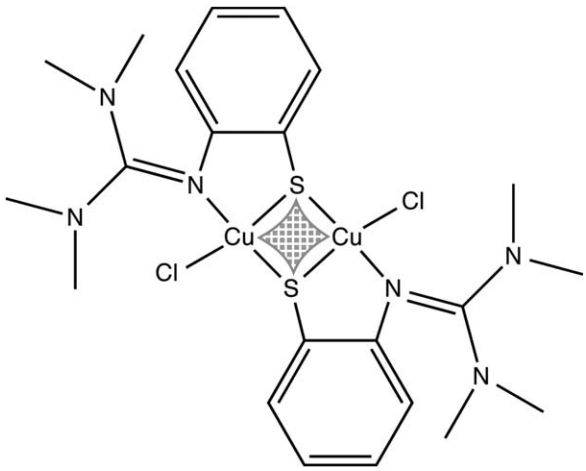

Figure 1. Schematic representation of neutral copper(II) thiolate species **1** reported in Ref. [45]. The "diamond" core is indicated by the gray diamond square.

starting point for the development of realistic Cu_A model complexes. The X-ray crystallography shows a folded structure with mirror symmetry with a rhombic, but puckered Cu_2S_2 diamond core. In analogy to similar systems with diamond core,[46–48] the properties of the complex are determined by the exchange coupling of the Cu and S atoms[49] by which the ground state is composed of a multideterminant wave function. In the framework of density functional theory (DFT), this wave function is not directly accessible. But Noodleman[50–53] showed that its total energy can be approximated by a *so-called* broken symmetry (BS) calculation in which an antiferromagnetic configuration is postulated* and used to calculate the singlet–triplet total energy splitting.

In this study, the BS approach within DFT is used to explore the molecular geometry and electronic structure of the neutral complex. This article is organized as follows: After a brief description of the computational method, the energy landscape within the BS configuration is investigated, addressing the question of the structural ground state and whether there are other possible metastable or degenerated minima. Afterward, technical aspects are discussed, focusing on the difference between the gas and the solid phase, the role of the van der Waals interaction (dispersion), and the choice of the exchange–correlation (XC) functional. The next two sections provide an in-depth analysis of the exchange coupling of the antiferromagnetic BS configuration by which the coupling constants are calculated with the help of two different spin decontamination schemes and used afterward to reconstruct the total energy curve of the multideterminant singlet state. The atomic charges are subsequently analyzed regarding the question of the valency. Finally, the orbital character and spatial distribution of the highest occupied molecular orbital (HOMO) and lowest unoccupied molecular orbital (LUMO) are discussed, suggesting the reduced, that is negatively charged complexes as a possible starting point for the development of realistic Cu_A model complexes.

*Although the structural symmetry is retained, the asymmetry of the spin degrees of freedom "breaks" the symmetry of the wave function.

Computational Method

The structurally and electronically relaxed minimum energy state of **1** and its bromo derivative **2** are determined within DFT. The multideterminant character of the neutral ground state is covered by the BS approach.[50–54] We use both the Gaussian09 code,[55] using localized basis functions, and the Quantum ESPRESSO package[56] which is based on a plane-wave (pw) representation of the electronic orbitals. An infinite number of pws forms a complete set, and a pw basis converges in a smooth, monotonic manner to the target wave function. The convergence of the calculation can easily be monitored and controlled by varying the pw cutoff, allowing to approach the completeness of the basis set and thus to eliminate related numerical errors. Using norm-conserving pseudopotentials, an energy cutoff of 90 Rydberg is found to lead to converged results for the systems studied here. In addition, as the pw basis functions are not associated with any particular atom, pw basis sets do not lead to basis set superposition errors and are ideally suited for modeling periodic boundary conditions appropriate for molecular crystal calculations. At the same time, cc-pVDZ and cc-pVTZ basis sets[57–59] are used in the Gaussian calculations. Hence, a strict scf convergence criterion of 10^{-10} Hartree as well as tight convergence criteria for relaxations are enforced. The electron–electron interaction is modeled here with various local, semilocal, and nonlocal XC functionals. Although, from a purist's point of view, functionals with as few parameters as possible are clearly desirable,[60] they are not always expedient for complexes including transition metal atoms like copper. Therefore, we compare the results obtained within the local-density approximation (LDA),[61–63] the Perdew, Burke, and Ernzerhof (PBE) implementation of the generalized gradient approximation (GGA)[64] as well as the hybrid B3LYP[65–67] and TPSSh functionals[68–70] which incorporate some Hartree–Fock exchange. The latter functional depends explicitly on the kinetic energy density of the occupied one-particle orbitals and has shown a superior performance in various recent studies on transition-metal systems (for a detailed discussion, see Ref. [71]).

Although the ubiquitous dispersion interaction can be accounted for by performing high-level quantum-chemical wave function or quantum Monte Carlo methods or by the combination of exact exchange plus correlation energy within the adiabatic-connection fluctuation–dissipation theorem,[72] it is neglected by most of the currently used XC functionals in DFT calculations. Among the many concepts to include dispersion interaction in DFT,[73–75] the addition of a pairwise interaction energy $\sim C_6R^{-6}$ with a suitable cutoff function for small atomic distances R (Refs. [76–78]) is a computationally particularly inexpensive, still often rather accurate approach.[79,80] This so-called DFT-D scheme delivers information on the influence of vdW forces at virtually no additional computational costs in an *a posteriori* way. In this study, we employ this scheme using the DFT-D2 and D3BJ parameter sets proposed by Grimme et al.[81,82] for studying the impact of dispersion effects on the molecular properties.

To probe the influence of the spin–orbit coupling (SOC) on the energetic and electronic properties of the investigated

copper disulfide complexes as well as to study the possible relevance and influence of noncollinear spin orientation,[83] we perform calculations starting from the Foldy–Wouthuysen transformed[84] Dirac Hamiltonian within the zero-order regular approximation (ZORA).[85] As we have shown earlier for a series of transition-metal systems,[86] SOC may be accounted for by an additional contribution to the nonlocal part of *scalar-relativistic* PAW pseudopotentials. This approach, described in detail in Ref. [87], allows for accurate, but numerically highly efficient relativistic calculations including SOC for spatially anisotropic potentials and is applied here to the species **1** in the gas phase.

Results and Discussion

Energy landscape within the BS approach

At first, we address the energetics of the neutral complex via BS calculations; we determine the geometry of the BS configuration and search for alternative metastable minima and saddle points, both with possible relevance for the synthesis. For this purpose, we start scanning the two-dimensional potential energy surface (PES) for the system in antiferromagnetic electronic configuration, that is for a Hilbert space with vanishing total spin $S = 0$, built up from wave functions that give rise to a vanishing total magnetic moment

$$m_{\mathrm{tot}} = \int (n_\alpha(\vec{r}) - n_\beta(\vec{r}))\, d^3r = N_\alpha - N_\beta = 2S \qquad (1)$$

but specific absolute magnetic moment

$$m_{\mathrm{abs}} = \int |n_\alpha(\vec{r}) - n_\beta(\vec{r})|\, d^3r. \qquad (2)$$

Here, $n_\alpha(\vec{r})$ and $n_\beta(\vec{r})$ denote the charge density of the corresponding spin channels α and β, respectively. Their difference $m(\vec{r}) = n_\alpha(\vec{r}) - n_\beta(\vec{r})$ is often called magnetization density.

For the PES, the Cu—Cu and S—S distances are chosen as parameters. Hence, the complex was structurally fully relaxed for specific constrained Cu—Cu and S—S distances, sampled on a dense mesh. The result, on the PBE+D2/pw level of theory, is shown in Figure 2. Earlier DFT calculations on other Cu_A model complexes identified two flat minima that can be rationalized by two types of ground state wave functions, σ_u^* and π_u that correspond to shorter and longer Cu—Cu distances.[88,89] Two distinct Cu—Cu distances, corresponding to two different Cu oxidation states, characterize as well the Cu_2O_2 binding motif in many model complexes for the binuclear copper enzyme tyrosinase; for example, see Refs. [90–94], where the short- and long-distance copper configuration are referred to as oxo and peroxo isomers. In all these cases, the overall flat geometry of the rhombic dicopper core remains intact, and different Cu—Cu distances are accommodated by varying the bonding angles. However, this is different for **1**: Besides the ground state with a rhombic, but puckered Cu_2S_2 core with a Cu—Cu distance below 2.9 Å and a S—S distance of about 3.3 Å, no further minimum with the same kind of geometry is found. There is, however, a metastable conformer with a "flat core" with inversion symmetry $\mathbf{1}^{\mathrm{inv}}$, 8.95 kcal/mol (388 meV) higher in energy (Fig. 3c), as well as another metastable minimum **1*** lying 13.88 kcal/mol (602 meV) above **1** on the PES (Fig. 2). The latter corresponds to a Cu—Cu distance of 3.7 Å and a S—S distance of 2.2 Å. It still reflects mirror symmetry, but the rhombic geometry of the Cu_2S_2 core is lost, and the system adopts an end-on geometry with a sulfur bridge (compare Fig. 3b). This metastable isomer **1*** is reached if the S—S distance is reduced below about 2.4 Å and results from the relief of the corresponding intramolecular strain. Interestingly, the S—S bridge found in **1*** is reminiscent of the educts in the synthesis leading to **1**.[45] In Figure 2b, the absolute magnetic moment m_{abs} of **1** calculated within PBE+D2/pw is shown in dependence on the Cu—Cu and S—S distance for the relaxed molecular structures discussed above. It should be noted that in contrast to the total magnetic moment m_{tot}, which vanishes by definition for all investigated BS configurations, m_{abs} is

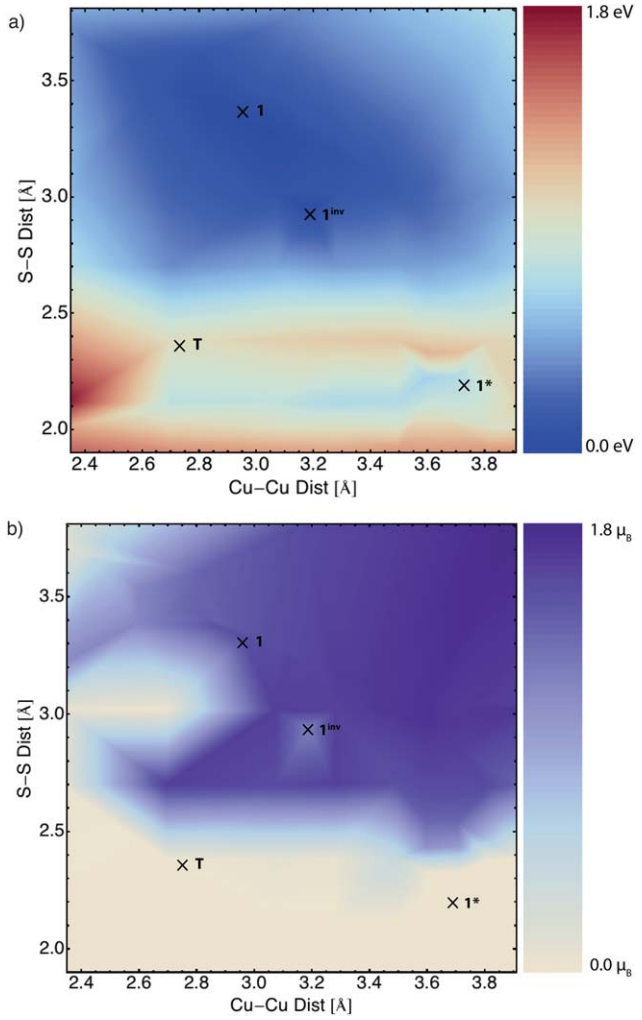

Figure 2. Calculated (PBE+D2/pw, BS approach) two-dimensional PES a), normalized to the minimum energy configuration (labeled **1**). Also shown is the corresponding absolute magnetic moment [eq. (2)] b). Metastable minima within mirror and inversion symmetry are marked by **1*** and $\mathbf{1}^{\mathrm{inv}}$, respectively (see also Figs. 3b and c), whereas **T** denotes a possible transition state between **1** and **1***.

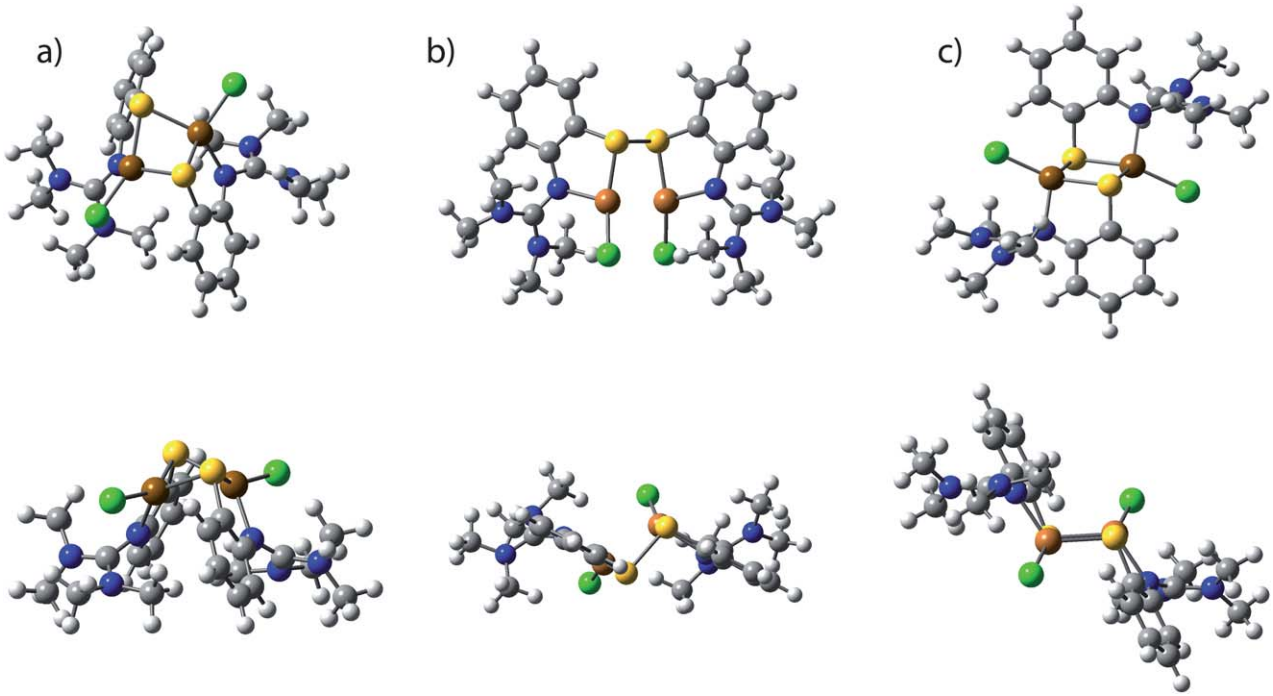

Figure 3. Calculated (structurally relaxed via PBE+D2/pw) geometries of the neutral $Cu_2(NGuaS)_2Cl_2$ complex as indicated in the PES shown in Figure 2: Besides the stable **1** a) and metastable **1*** b) states with mirror symmetry and puckered Cu_2S_2 diamond core, also a metastable ("flat core") configuration within inversion symmetry $\mathbf{1}^{inv}$ c) is shown.

strongly varying depending on the molecular arrangement. In contrast to the minimum total energy structure **1**, the metastable minimum **1*** provides a diamagnetic singlet where both the total [eq. (1)] and the absolute [eq. (2)] magnetic moments vanish. Generally, the magnetic moment tends to decrease or even to vanish for short S—S distances (Fig. 3b).

Molecular structures—gas phase versus solid state

To discuss the influence of different XC functionals, we compare key structural parameters of the Cu_2S_2 core (Figs. 1 and 3a) calculated for various functionals and basis sets with the experimental values which, however, correspond to X-ray diffraction data obtained for the solid state. The experimental error bars for the Cu, S, and Cl bond lengths/angles are 0.0007 Å/0.006°, respectively,[45] which is clearly below the numerical accuracy of the present calculations. The results are summarized in Table 1.[47] To explore the crystallization effects on the molecular structure and energy of **1**, Table 1 contains besides the gas-phase data, also the results for the solid state ("PBE/pw" and "PBE+D2/pw"). Hence, periodic boundary conditions have been used to model the molecular crystal with a two-molecule unit cell as shown in Figure 4.

Interestingly, gas-phase molecule calculations performed with the LDA yield structural parameters that are largely in close agreement with the experiment. Nevertheless, with LDA a proper BS configuration cannot be stabilized, falling back to an unlikely closed shell configuration. The GGA within PBE leads to bond lengths that are larger than the results of LDA by 0.1–0.3 Å. Very often (Refs. [76,77]), large structural differences between LDA and GGA calculations are indicative for a strong influence of dispersion interactions that frequently are fortuitously mimicked by the former. Hence, the influence of dispersion interaction is explored here in more detail. For the calculation with a pw basis set, we use the DFT-D2 scheme.[81,95] From the comparison of the results for the vacuum molecule and the solid (Table 1), it becomes obvious that the dispersion interaction plays only a minor role for the latter. This can be explained by the solid-state matrix, leading to some cancellation of van der Waals forces. This is, of course, not the case for the isolated gas-phase complex. Owing to the folded geometry of **1**, the face-to-face ligands sense a noticeable dispersion attraction that increases the S—Cu—S angle, resulting in a larger S—S bond and shortening the Cu—Cu distance. Hence, the PBE+D2 molecular structures calculated for the gas-phase and solid-state embedded species do not differ more than a couple of hundredths of Ångstrom. The fact that there are still large discrepancies compared to the measured geometry is, thus, indicative for an insufficient theoretical modeling rather than for large differences between gas-phase and solid-state geometry.

The choice of the XC functional

Therefore, we explore the influence of the exact exchange contribution to the XC functional in the following. We expand the wave functions in a localized basis (cc-pVDZ and cc-pVTZ) rather than pws to keep the numerical effort as low as possible. For technical reasons, the Becke–Johnson damping (D3BJ) scheme[82] was used to model the dispersion interaction in

Table 1. Calculated key structural parameters (bond lengths in Å, angles in °) and the absolute magnetic moment m_{abs} (in μ_B) [eq. (2)] in comparison with the experimental data.[a] For comparison, the values of the bromo derivative **2** are also given (lower part).

	Cu—Cu	S—S	Cu—Cl/Br	Cu—S	Cu—S	∢ (Cu—S—Cu)	∢ (S—Cu—S)	m_{abs}
Exp. [45] (solid state)	2.73	3.19	2.22	2.22	2.34	73.69	88.96	–
LDA/pw	2.71	3.21	2.19	2.18	2.26	75.06	92.46	0
PBE/pw	3.03	3.27	2.27	2.27	2.39	80.93	89.06	1.53
PBE/pw (solid state)	2.88	3.30	2.28	2.27	2.41	75.82	89.50	1.33
PBE+D2/pw	2.90	3.31	2.26	2.28	2.38	76.78	90.39	1.40
PBE+D2/pw (solid state)	2.88	3.31	2.28	2.29	2.41	75.59	89.42	1.31
PBE+D2/pw (singlet)	2.82	3.35	2.26	2.27	2.37	74.86	92.31	0
PBE+D2/cc-pVDZ	2.75	3.34	2.23	2.27	2.36	73.02	92.28	0
PBE+D3BJ/cc-pVDZ	2.73	3.34	2.23	2.26	2.34	72.75	92.97	0
PBE+D3BJ/cc-pVTZ	2.74	3.31	2.23	2.24	2.33	73.63	92.84	0
PBE+D3BJ/aug-cc-pVTZ	2.82	3.30	2.24	2.25	2.35	75.64	91.64	0.57
B3LYP/cc-pVDZ	3.14	3.22	2.25	2.30	2.41	83.39	86.15	1.91
B3LYP/cc-pVTZ	3.14	3.19	2.25	2.28	2.40	84.03	85.58	1.92
B3LYP+D3BJ/cc-pVDZ	3.00	3.25	2.24	2.30	2.39	79.18	87.49	1.87
B3LYP+D3BJ/cc-pVTZ	2.95	3.25	2.23	2.28	2.39	78.66	88.58	1.87
TPSSh/cc-pVDZ	2.94	3.22	2.24	2.28	2.37	78.25	87.62	1.79
TPSSh/cc-pVTZ	2.94	3.17	2.23	2.26	2.36	79.14	86.73	1.81
TPSSh+D3BJ/cc-pVDZ	2.78	3.27	2.23	2.28	2.35	73.86	90.08	1.71
TPSSh+D3BJ/cc-pVTZ	2.78	3.24	2.22	2.26	2.33	74.39	89.92	1.71
Exp.[b] (solid state)	2.71	3.19	2.35	2.22	2.33	73.12	89.19	–
PBE+D2/pw	2.88	3.33	2.39	2.29	2.38	76.13	91.17	1.31
PBE+D2/pw (solid state)	2.84	3.32	2.42	2.29	2.41	74.34	89.83	1.25
TPSSh+D3BJ/cc-pVDZ	2.76	3.29	2.37	2.28	2.34	73.48	90.55	1.67

[a] So far, m_{abs} could not be determined experimentally. [b] A. Neuba, G. Henkel, Private communication, 2014.

these calculations. The difference to the D2 results is expected to be of minor importance. However, strong changes are induced by the hybrid functionals. The frequently used B3LYP approximation deteriorates rather than to improve the agreement between experiment and theory: Irrespective of whether or not dispersion is included and if a cc-pVDZ or cc-pVTZ basis is used, the Cu—Cu distance is severely overestimated, by up to 0.4 Å. In accordance with former calculations for other Cu_4-like complexes by Takano et al.,[96] a substantially improved modeling is achieved if the meta-GGA is combined with 10% of Hartree–Fock exchange in the TPSSh functional, leading to 0.2 Å shorter Cu—Cu distances. Dispersion interaction shortens the bond lengths further, apart from the S—S distance, which even slightly expands. This is related to the folded geometry of **1** (Fig. 3a): The face-to-face ligands sense a large dispersive attraction that increases the S—Cu—S angle and stretches the S—S bond length beyond its measured value. The resulting butterfly opening of the diamond core has an angle of 124°.

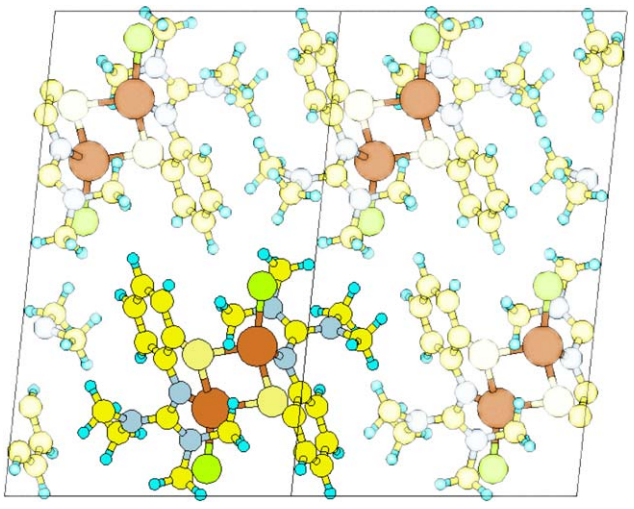

Figure 4. Schematic representation of the crystalline structure of **1** and **2** with a two-molecule unit cell (one highlighted) as derived by X-ray diffraction in Ref. 45. It should be note that for **1** a more complicated structure with four molecules in the unit cell (two of them inverted and shifted by 50% of the lattice constant) is determined. [Color figure can be viewed in the online issue, which is available at wileyonlinelibrary.com.]

In Figure 5 the influence of the XC functionals, the molecular modeling, and the dispersion interaction are further shown by the one-dimensional PESs for selected calculation schemes: TPSSh+D3BJ/cc-pVDZ, B3LYP+D3BJ/cc-pVDZ, and PBE+D2/pw. Also, shown are PBE+D2/pw calculations for the molecular crystal that employ periodic boundary conditions. The respective calculations are performed assuming restricted closed shell (diamagnetic), triplet (paramagnetic), and BS (antiferromagnetic) configurations. Their total energies are given in dependence on the Cu—Cu distance exclusively, whereas relaxing all other degrees of freedom. For all calculation schemes, a BS configuration with nonvanishing absolute magnetic moment m_{abs} gives the lowest energy. Nevertheless, as already found in Refs. [97–100] for similar systems, the extent to which the BS or triplet configuration is lowered in total energy with respect to the closed shell configuration scales with the amount of Hartree–Fock exchange employed in the calculation. It is important to mention, though, that the restricted closed shell configuration has no chemical meaning for the ground state. Nevertheless, the corresponding energy curves are illustrative in showing that for small Cu—Cu distances the BS solution converges (depending on the different functionals) into the chemically unlikely closed shell solution (Fig. 5).

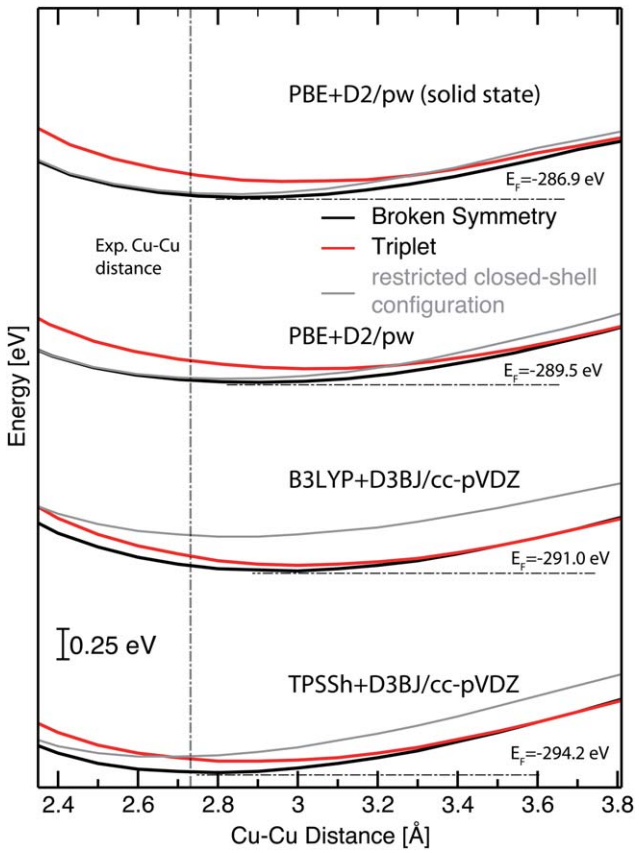

Figure 5. One-dimensional PESs for different spin configurations and XC functionals. For each BS energy minimum, the formation energy E_F is given; the vertical line indicates the experimental Cu—Cu distance from Ref. 45. The gray line indicates the hypothetical closed shell singlet energy shown here for comparison. [Color figure can be viewed in the online issue, which is available at wileyonlinelibrary.com.]

Taken together, the TPSSh+D3BJ/cc-pVDZ calculations within the BS approach result in a structure that essentially resembles the experimental findings. It can, thus, be used as a reliable basis for further investigations presented in the following section.

Antiferromagnetic coupling within the BS state

The BS state does not comprise the multideterminant character of the singlet ground state, but often yields a very good approximation for the correct ground state density. Nevertheless, the geometry of the multideterminant singlet differs slightly from that of the BS configuration as well.[54] Still, the BS approach provides a good estimate for the geometry and related spectroscopic properties as explained in Refs. 46,47,101–104. Steps beyond, however, require an in-depth analysis of spin system. Assuming that the BS configuration yields not only a reliable estimate for the geometry but for the spin distribution as well, we analyze the antiferromagnetic coupling within the BS state in terms of the two spin channels α and β. The fact that essentially the Cu and S atoms are affected by the spin asymmetry is illustrated by the calculated magnetization density $m(\vec{r})=n_\alpha(\vec{r})-n_\beta(\vec{r})$ as shown in Figure 6. The atoms of the diamond core are mostly responsible for the *absolute* magnetic moment and hence for the antiferromagnetic coupling. Around 75% originates equally from the Cu *d* states and S *p* states, 10% from the Cl and N(Gua) ligands, whereas the remaining part is distributed over the whole molecule. This asymmetry in the α and β spin distribution reduces the geometrical C_2 symmetry to $C_2{}^\circ\sigma_x$. Hence, the subsets of each spin channel of the Kohn–Sham (KS) orbitals $|\phi_j^\sigma\rangle_{\sigma=\{\alpha,\beta\}}$ are energetically degenerated. To rationalize the energy lowering owing to this symmetry reduction, we consider the contribution of the individual orbitals to the Hartree contribution

$$E_j^H=\frac{q}{2}\int\int\frac{n_j^\alpha(\vec{r})n_j^\beta(\vec{r}\,')}{|\vec{r}-\vec{r}\,'|}d^3r\,d^3r' \tag{3}$$

to the DFT total energy. For most of the orbitals, the corresponding Coulomb repulsion is found to be lower in case of the BS state than for the closed shell configuration. In total, this electronic reorganization leads to an energy that is 3.04 kcal/mol (132 meV) lower owing to the antiferromagnetic order (TPSSh+D3BJ/cc-pVDZ). Simultaneously, the HOMO–LUMO gap widens from 1.1 to 1.5 eV.

The antiferromagnetic coupling is reflected in a nonvanishing absolute magnetic moment m_{abs} [eq. (2)] of up to 1.92 μ_B calculated within B3LYP/cc-pVTZ. The corresponding value of the TPSSh+D3BJ/cc-pVTZ calculation, which closest resembles the experimental geometry, amounts to 1.71 μ_B. In this context, it is interesting to have a closer look at the PBE results. The combination of PBE with a pw basis results in a sizable absolute magnetic moment of 1.31–1.53 μ_B depending on whether or not dispersion interaction is included and if the calculations are performed for gas-phase or solid-state species. In contrast, unless the basis is augmented to a triple-Zeta basis including diffuse functions, the PBE description with localized basis sets does not show any stable antiferromagnetic minimum energy configuration and relaxes barrier-free into the diamagnetic closed shell configuration. This indicates that localized basis sets in combination with (semi-) local functionals are, in this particular case, not suitable to represent the electronic BS state. It is furthermore possible that the frozen-core pseudopotential approach profits from error cancellation. The majority of the results, in any event, point to a BS minimum energy configuration with a nonvanishing absolute magnetic moment of about $m_{\text{abs}} \approx 1.4$–$1.9$ μ_B.

All the calculations discussed above rest on the assumption of a perfectly aligned, collinear spin orientation. To explore a possible influence of noncollinear spin polarization, we perform relativistic two-component PBE/pw calculations for isolated molecular species that include SOC and allow for arbitrary spin orientations.[87] It is found, however, that irrespective of the spin orientation used as starting configuration, the spin degrees of freedom relax into a collinear configuration with all spins aligned along the direction imposed by the Cu magnetic moment (Fig. 6). Hence, the orientation of the quantization axis is almost arbitrary: The corresponding energy difference is below 10^{-6} eV, suggesting a very efficient intramolecular antiferromagnetic coupling. The inclusion of SOC is

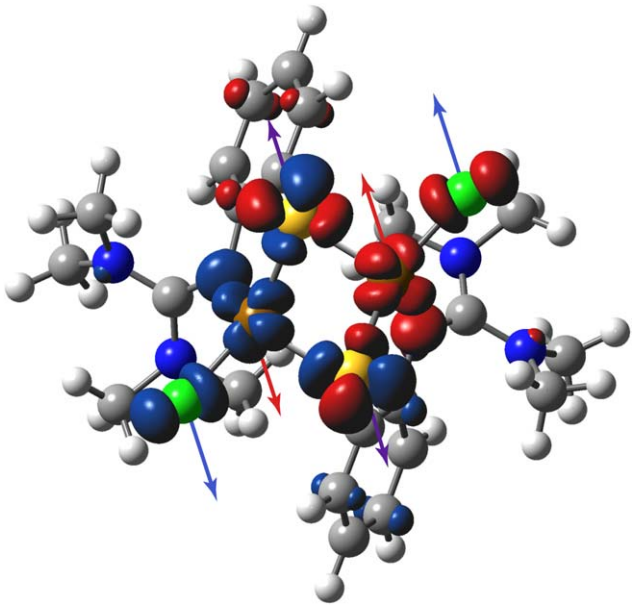

Figure 6. Calculated (PBE/pw) BS magnetization density $n_s(\vec{r})=n^{\alpha}(\vec{r})-n^{\beta}(\vec{r})$ for the minimum energy state of **1** (red, positive; blue, negative). Arrows indicate the corresponding local spin orientation. For clarity, the arrows are scaled equally and are only shown for local magnetic moments of >0.001 μ_B. [Color figure can be viewed in the online issue, which is available at wileyonlinelibrary.com.]

also of minor influence (<1 meV) for the relative stability of the different spin states of the isolated molecular species. We cannot exclude, however, a more significant influence in molecular crystals, in particular in case of **1**, where four molecules in a hexagonal unit cells[45] give various possibilities for a rather complicated spin ordering. This is, however, beyond the scope of this article in which full relativistic calculations are restricted to the isolated molecular species.

Exchange coupling

The exchange coupling within the BS configuration can be analyzed with respect to the phenomenological Heisenberg–Dirac–van Vleck Hamiltonian[105]

$$\hat{H}=-2J\,\hat{S}_1\cdot\hat{S}_2 \tag{4}$$

Experimentally, the exchange coupling constants are related to the temperature dependence of the magnetic susceptibilities. In Ref. [45], this has been measured for powder samples of **1** and **2** using a SQUID magnetometer. From the data of the bromo derivative **2**, a magnetic phase transition at 160 K can be clearly determined, resulting in an experimental value of $|2J_{\mathbf{2}}|=2210\ \mathrm{cm}^{-1}$.[45] For **1**, a very strong antiferromagnetic coupling of the two Cu atoms is concluded: As no clear transition is observed up to 290 K, the coupling constant $|2J_{\mathbf{1}}|$ might be $>4000\ \mathrm{cm}^{-1}$, that is considerably larger than $|2J_{\mathbf{2}}|$. Apart from the coupling constant, however, the electronic and structural properties of the molecular species **1** and **2** do not differ significantly (Table 1). To understand this behavior, we calculate the coupling constant J from the energies and spin expectation values of the corresponding high-spin (HS, triplet) and BS configurations by following Ref. [106]

$$J=\frac{E_{\mathrm{BS}}-E_{\mathrm{HS}}}{\langle\hat{S}^2\rangle_{\mathrm{HS}}-\langle\hat{S}^2\rangle_{\mathrm{BS}}}, \tag{5}$$

which in the weak and strong bonding limits can be reduced to simpler formulas alternatively used in the literature.[51,52,107,108] We note that the experimental data for J were obtained from crystalline samples. It has been pointed out earlier that the calculated coupling constants are very sensitive with respective to the molecular geometries.[47] Therefore, in Table 2, we summarize the data calculated for the measured ground-state geometries as well for relaxed molecular structures, assuming in both cases a vertical, atomic structure conserving, spin excitation.

For HS states, the spin expectation value $\langle\hat{S}^2\rangle_{\mathrm{HS}}$ in terms of $\hbar^2$ will be close to integer $S(S+1)$. The calculation of $\langle\hat{S}^2\rangle_{\mathrm{BS}}$ for a BS state is more involved. Owing to serious spin contamination,[109,110] the corresponding BS wave function is by no means an eigenfunction of $\langle\hat{S}^2\rangle$. The total spin angular momentum is *two-particle* in nature. Hence, in the framework of DFT, a relationship to the (magnetization) density or at least the KS *one-particle* orbitals have to be established by modeling the exchange–correlation hole. Several methods are used in the literature.[111–114] In the so-called "noninteracting" (NI) scheme, the expectation value is obtained by evaluating the overlap integrals between spin-up and spin-down electrons[109,110]

$$\langle\hat{S}^2\rangle_{\mathrm{NI}}=\hbar^2\left[S(S+1)+N_\beta-\sum_{i=1}^{N_\alpha}\sum_{j=1}^{N_\beta}\left|\int\phi_{i,\alpha}^{\mathrm{KS}}(\vec{r})\phi_{j,\beta}^{\mathrm{KS}}(\vec{r})d^3r\right|^2\right]. \tag{6}$$

This approach can be used to rationalize the antiferromagnetic coupling by defining a pair of magnetic orbitals which account completely for the overlap.[112] As there is, however, no formal justification for describing the exchange–correlation hole via KS orbitals, and for correlating the expectation value $\langle\hat{S}^2\rangle$ with the absolute magnetic moment of the antiferromagnetically coupled BS state (Table 1), we compare the results of the NI scheme with the prediction of an *exchange*-only local spin *density* (XLSD, or shorter XD) approach[115]

$$\langle\hat{S}^2\rangle_{\mathrm{XD}}=\hbar^2\left[S(S+1)-\int_{n_s<0}n_s(\vec{r})\,d^3r\right], \tag{7}$$

where $n_s(\vec{r})=n_\alpha(\vec{r})-n_\beta(\vec{r})$ denotes the local magnetization density (Fig. 6). Exploiting that on the one hand

$$-\int_{n_s<0}n_s(\vec{r})\,d^3r=\int_{n_s<0}|n_s(\vec{r})|\,d^3r,$$

and on the other hand

$$2\cdot\int_{n_s<0}|n_s(\vec{r})|\,d^3r=\int_{\infty}|n_s(\vec{r})|\,d^3r-\int_{\infty}n_s(\vec{r})\,d^3r=m_{\mathrm{abs}}-m_{\mathrm{tot}},$$

Table 2. Calculated and measured exchange coupling constants, here given by the singlet–triplet splittings $2J$ in cm^{-1}[a].

	Exp. geometry		Calc. geometry	
	1	**2**	**1**	**2**
Experiment [45]		−2210		
PBE+D2/pw	−1910	−1960	−1818	−1898
PBE+D2/pw (solid)	−2210	−2241	−1901	−1886
B3LYP+D3BJ/cc-pVDZ	−1286	−1331	−875	−925
TPSS+D3BJ/cc-pVDZ	−1834	−1941	−2228	−2300
TPSSh+D3BJ/cc-pVDZ	−1541	−1591	−1637	−1641

[a] Using the NI spin-decontamination scheme, the calculations are performed for different functionals, using either the experimental (X-ray diffraction) or the respective calculated geometries of $Cu_2(NGuaS)_2Cl_2$ (**1**) and $Cu_2(NGuaS)_2Br_2$ (**2**).

and furthermore using the definitions of the absolute and total magnetic moments in eqs. (1) and (2), respectively, one can rewrite eq. (7) as

$$\langle \hat{S}^2 \rangle_{XD} = \hbar^2 \left[S(S+1) + \frac{m_{abs}}{2} - S \right]. \quad (8)$$

In other words, $m_{abs}/2 - S$ can be rationalized as an estimate for the spin contamination in DFT. In Table 3, the $\langle \hat{S}^2 \rangle$ values obtained via eqs. (6) and (8) are compared. The XD approach gives the values that are always larger than the KS orbital-based results of the NI approach, and hence the difference becomes smaller for larger spin contaminations. Cohen et al.[110] have elaborated a gradient corrected density functional for $\langle \hat{S}^2 \rangle$, which lowers the results correcting for spin contamination. The same trend should be expected if correlation is taken into account. The XD results can, thus, be seen as an upper limit for $\langle \hat{S}^2 \rangle$, those of the NI approach as a lower one. The difference of the expectation value used to calculate J comes again closer to each other, and the chosen method only moderately affects the resulting coupling constants. In addition, formula (5) is believed to lead to slightly underestimated singlet–triplet splittings $|2J|$.[116,117] Hence, the NI–KS orbital-based method according to eq. (6) allows to take advantage of error cancellation and can be trusted to give reasonable estimates for the coupling constants J.

As summarized in Table 2, the calculated coupling constants depend critically on the modeling of the DFT functional. First, we discuss coupling constants obtained for molecular species in the gas phase using the experimental geometries from X-ray crystallography: The calculations based on the semilocal PBE and on the TPSS/cc-pVDZ meta-DFT functional, both containing no exact exchange, give very similar results with comparatively large $|J|$ values. The smallest coupling constants, for both **1** and **2**, are obtained within B3LYP/cc-pVDZ; the values for the TPSSh functional with a medium content of exchange are in between. This behavior reflects the varying energy differences between the BS and the triplet states, which in turn are related to the fact that functionals with a larger amount of Hartree–Fock exchange tend to favor HS states.[97–100] As for all functionals the values are underestimated, best agreement with experiment is obtained for the semilocal functionals, which in case of the bromo derivative **2** is still about 10% smaller than the experimental value. A possible source for serious uncertainties is the influence of intermolecular (lattice) interactions in the molecular crystal.

To investigate the influence of such crystallization effects, additional total energy calculations (on the PBE/pw level of theory) were performed for the solid phase. In comparison to the gas-phase, larger energy differences between the BS and the triplet HS states are obtained (Fig. 5), whereas the difference of the corresponding $\langle \hat{S}^2 \rangle$ expectation values increases only slightly (Table 3). As a consequence larger exchange couplings (by ∼10%) are predicted for the solid state. For **2**, where experimentally a transition into a ferromagnetic configuration has been clearly observed, the resulting exchange splitting of $-2240\ cm^{-1}$ (278 meV) agrees very well with the experimental value of $-2210\ cm^{-1}$ (Table 2). For **1**, however, we obtain almost the same exchange coupling constant. This seemingly contradicts the experimental finding that the singlet–triplet splitting $|2J_1|$ for **1** should be considerably larger than the value $|2J_2| = 2210\ cm^{-1}$ for the bromide derivative **2**. One has to mention, however, that the calculated coupling constants J are strongly geometry dependent. They vary considerably if calculated minimum total-energy geometries are used instead of the experimentally observed crystal structures (cf. right part of Table 2). However, this effect cannot explain the large discrepancy in case of **1**. Owing to the strong similarities of all structural, electronic, and magnetic properties of the individual molecular species **1** and **2**, we might expect the differences in the molecular crystal lattice and their influence onto the spin-coupling as a possible origin: Although **2** crystallizes with two molecules in a regular unit cell, complex **1** crystallizes in a hexagonal cell containing four molecules. We

Table 3. Expectation values $\langle \hat{\boldsymbol{S}}^2 \rangle$ (in $[\hbar^2]$) for the triplet (HS) and the BS states as well as their difference $\Delta = \langle \hat{\boldsymbol{S}}^2 \rangle_{HS} - \langle \hat{\boldsymbol{S}}^2 \rangle_{BS}$ calculated for the Cl and Br derivatives (1 and 2) via the NI scheme [eq. (6)] and via the exchange-only (local) density approximation (XD, eq. (8)) for different functionals and geometries.

	1 BS		1 HS (triplet)		1(HS–BS)		2 BS		2 HS (triplet)		2(HS–BS)	
	$\langle \hat{S}^2 \rangle_{NI}$	$\langle \hat{S}^2 \rangle_{XD}$	$\langle \hat{S}^2 \rangle_{NI}$	$\langle \hat{S}^2 \rangle_{XD}$	Δ_{NI}	Δ_{XD}	$\langle \hat{S}^2 \rangle_{NI}$	$\langle \hat{S}^2 \rangle_{XD}$	$\langle \hat{S}^2 \rangle_{NI}$	$\langle \hat{S}^2 \rangle_{XD}$	Δ_{NI}	Δ_{XD}
PBE+D2/pw	0.53	0.77	2.007	2.11	1.48	1.34	0.46	0.65	2.007	2.11	1.55	1.46
PBE+D2/pw (solid)	0.47	0.67	2.006	2.06	1.54	1.39	0.43	0.63	2.006	2.10	1.57	1.47
B3LYP+D3BJ/cc-pVDZ	0.90	0.96	2.010	2.14	1.11	1.18	0.88	0.93	2.010	2.14	1.13	1.21
TPSS+D3BJ/cc-pVDZ	0.26	0.47	2.004	2.09	1.74	1.62	0.12	0.32	2.004	2.08	1.88	1.76
TPSSh+D3BJ/cc-pVDZ	0.76	0.86	2.008	2.13	1.25	1.27	0.73	0.83	2.002	2.13	1.27	1.30

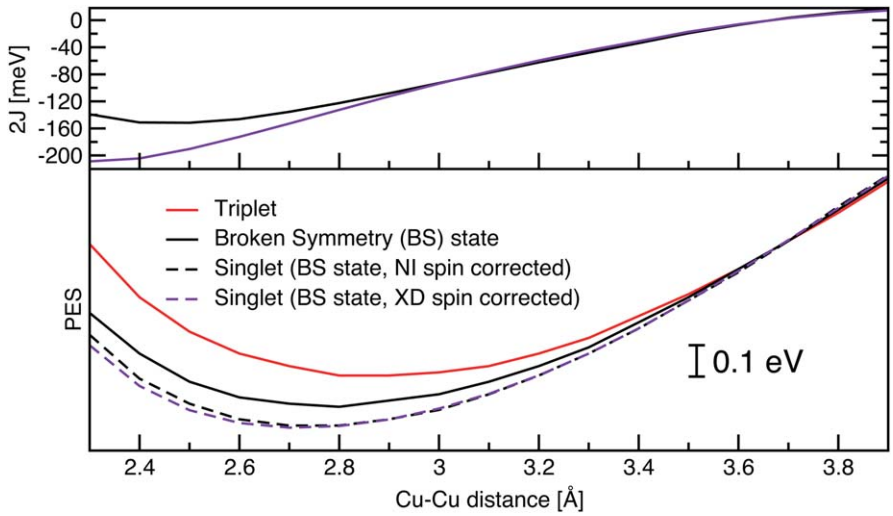

Figure 7. Top: Singlet triplet splitting factor 2*J* according to eq. (9) within the NI (black) and XD (purple) correction scheme. *Bottom*: One-dimensional PES for the triplet, BS, and multideterminant singlet configurations. Both calculations were carried out on the TPSSh+D3BJ/cc-pVDZ level of theory. [Color figure can be viewed in the online issue, which is available at wileyonlinelibrary.com.]

cannot exclude that thermal effects onto the molecular crystal structure and the spin-coupling therein actually lead to a suppression of a magnetic phase transition. Here, further experimental investigations for higher temperatures would be helpful. Based on the present results, we can conclude that the coupling constants are very sensitive to the details of the molecular structure and the interaction with neighboring molecules. This is especially seen in the case of **1**$^{inv:}$ Though the absolute magnetic moment is reduced to $m_{abs}=1.53\,\mu_B$ (Fig. 2b) along with $\langle S^2\rangle_{NI}=0.69$, the absolute value of the coupling constant increases to $|2J_{1^{inv}}|=2002\ cm^{-1}$ owing to the frustration of the triplet state (TPSSh+D3BJ/cc-pVDZ). Further improved theoretical results may, therefore, require (i) the use of the TPPSh functional in the solid-state calculation, (ii) the investigation of noncollinear spin ordering in the molecular crystal lattice, and (iii) the inclusion of thermal effects on the molecular crystal structure.

Nevertheless, already on the present level of theory, we are able to construct the total energy curve of the multideterminant singlet E_S with the formula by Yamaguchi et al.[118] which can be written as

$$E_S=E_{HS}+\frac{\langle S^2\rangle_{HS}}{\langle S^2\rangle_{HS}-\langle S^2\rangle_{BS}}(E_{BS}-E_{HS})=E_{HS}+\underbrace{\langle S^2\rangle_{HS}}_{\approx 2}J. \qquad (9)$$

For TPSSh+D3BJ/cc-pVDZ, the energy splitting and the one-dimensional PES are shown in Figure 7. Irrespective of whether the NI or XD scheme is used, the correction is maximal for short Cu—Cu distances (76 and 104 meV, respectively). At the minimum energy configuration, both methods shift the BS energy by about 64 meV downward, and the Cu—Cu distance is slightly reduced to 2.75 and 2.70 Å for the NI and XD scheme, respectively. Having in mind that the two schemes provide upper and lower limits for the correct data, we obtain a perfect agreement with the experimental value of 2.73 Å. For the Br derivative **2**, an application of the correction schemes leads to a similar improvement, reducing the Cu—Cu distance by about 0.05 Å to the experimental finding of 2.71 Å.

Valency of the ground states

From the measured Cu—K edge absorption, it was proposed that **1** is a Cu(II) complex.[45] A natural bond orbital (NBO) charge analysis (TPSSh/cc-pVDZ) performed for a Cu atom in **1** results in a net positive *atomic* charge of 1.01 e (Table 4) which certainly corresponds rather to the lower limit for a formal Cu(II) complex[119,120] and might even be explained by a Cu(I) complex.[121] To put this result into further context, we perform comparative PBE/pw calculations for prototypical Cu(I) and Cu(II) compounds, namely bulk CuCl and $CuCl_2$ ionic crystals, where the oxidation state is well defined, given by the stoichiometry, and compare the atom-projected charge distributions. The results compiled for different functionals are also summarized in Table 4. An accurate description of the Cu(II)Cl_2 electronic structure is, however, not trivial.[122,123] Nevertheless, using a noncollinear spin treatment (Computational Method section), the ground-state spin wave has been reproduced in the present calculations. The atomic base-projected Cu net charge as well as the projection of the total charge on the Cu 3*d*, 4*s*, and 4*p* states for the Cu(I)Cl and Cu(II)Cl_2 ionic crystals in Table 4 can be used as a reference for molecular Cu complexes. Here, the net charge of the 3*d* shell for Cu(II)Cl_2 is 0.50 e, whereas for Cu(I)Cl the charge deficiency is only 0.18 e. For all calculations, independent of the XC functional, the net charge of the 3*d* shell for **1** is between 0.40 and 0.53—close to that of Cu(II)Cl_2. From a comparison with hybrid DFT calculations, we estimate the error bars of these values to be below ±0.05 e. The same is found for the Br derivative **2**. Therefore, from an analysis of the *d*-shell occupation, it seems justified to

Table 4. Orbital projected charges (NBO analysis) for the ionic crystals Cu(I)Cl, $Cu(II)Cl_2$ (PBE/pw), and for **1** in the solid states (all PBE/pw) and the isolated complex **1** calculated with different functionals and basis sets (lower part of the table).[a]

		Cu					Cl				S			
		Δq	Total	3d	4s	4p	Total	3s	3p	3d	Total	3s	3p	3d
Cu(I)Cl	PBE/pw	0.86	10.80	9.82	0.32	0.68	7.18	1.58	5.04	0.56	–	–	–	–
$Cu(II)Cl_2$	PBE/pw	1.12	10.64	9.50	0.38	0.78	7.16	1.64	5.00	0.54	–	–	–	–
(Solid state)	PBE+D2/pw	0.99	10.95	9.48	0.53	0.94	7.59	1.78	5.44	0.36	6.09	1.50	4.02	0.55
	PBE+D2/pw	0.99	10.92	9.47	0.54	0.90	7.48	1.80	5.46	0.22	6.05	1.50	4.03	0.51
TPSS+D3BJ/cc-pVDZ		0.94	10.69	9.60	0.46	0.64	7.51	1.88	5.63	–	5.91	1.64	4.25	0.02
B3LYP+D3BJ/cc-pVDZ		1.03	10.53	9.53	0.44	0.56	7.53	1.88	5.65	–	6.00	1.66	4.32	0.02
B3LYP+D3BJ/cc-pVTZ		1.04	10.53	9.54	0.42	0.58	7.55	1.88	5.67	–	5.95	1.64	4.28	0.02
TPSSh+D3BJ/cc-pVDZ		1.01	10.59	9.55	0.44	0.60	7.53	1.88	5.74	–	5.94	1.64	4.28	0.02

Besides the net *atomic* charge $\Delta q = m + n$ of the Cu-atoms in $3d^{10-m}4s^{1-n}$ configuration, in particular the deviation m of the Cu 3*d* shell from a d^{10} closed shell occupation can serve as a reliable measure for the oxidation state.

classify **1** and **2** as Cu(II) complexes, in agreement with the previous interpretation of the X-ray absorption data.[45]

Alternative structures and reduced species

With the values between 2.7 and 2.8 Å, the calculated and the measured Cu—Cu distances of the neutral model complex **1** are significantly larger than the value of 2.44 Å typically reported for flat Cu_A centers.[1–3,14] As already mentioned above, complex **1** has a metastable conformer with C_i symmetry $\mathbf{1}^{inv}$ possessing a Cu_A typical, flat diamond core. On the TPSSh+D3BJ/cc-pVDZ level of theory, however, it is 8.95 kcal/mol (388 meV) higher in energy than the folded C_2 symmetry structure **1**, and features an even far longer Cu—Cu distance of 3.18 Å (Fig. 3c). Owing to the even number of electrons, neither the neutral complex **1** nor the $\mathbf{1}^{inv}$ can be mixed-valent as in Cu_A.

Therefore, we investigate the reduced (negatively charged) species of the abovementioned symmetry variants as a possible mixed-valent core. A DFT treatment is here much more straight forward as the $S = 1/2$ ground state of the negatively charged species is given by a single Slater determinant. After relaxing the structures of the reduced complexes, we find a structure with C_2 symmetry similar to **1** as most stable. The energy gain with respect to a structure with inversion symmetry (again similar to $\mathbf{1}^{inv}$), however, becomes smaller and now amounts to 5.37 kcal/mol (233 meV). In other words, the general structure of the diamond core remains qualitatively the same, irrespective of the charge state. The symmetry of the molecules is retained, and the oxidation state for the negative species becomes actually mixed-valent $[Cu^{1.5+}...Cu^{1.5+}]$ with the SOMO being primarily delocalized over the diamond core (Fig. 8). At the same time, the Cu—Cu distance is reduced to 2.82 Å ($\mathbf{1}^{inv}$) and 2.64 Å (**1**), respectively.

HOMO and LUMO orbital character

In the context of the electronic and spin-dependent properties of the neutral and negatively charged species of **1**, it is illustrative to analyze the orbital composition of the HOMO and LUMO as shown in Figure 9. The dependence on the basis set and on the XC functional is shown in Figure 10. We find only minor differences between the double-Zeta and the triple-Zeta basis set results. In contrast, the Cu contributions to the HOMO and LUMO depend strongly on the amount of exact exchange used in the functional: 20% of exact exchange in the B3LYP hybrid functional decreases the HOMO Cu contribution significantly (to the values of $<$15%). At the same time, the Cu contribution in the LUMO is increased, the HOMO–LUMO gap is enlarged (Fig. 10) and a higher magnetic moment is obtained (Table 1) .

On the TPSSh+D3BJ/cc-pVDZ level of theory (with 10% exact exchange), the LUMO for **1** comprises 40% Cu, 30% S, 9% Cl *p*, and 7% N states. For the Br derivative **2**, we obtain basically the same values. Only the contribution at the Br ligands (11%) is slightly increased, and hence that of the Cu atoms (38%) is decreased by the same amount. Despite the electron transfer from the sulfur to the additional Cl and Br ligands, the LUMO values are, thus, nearly identical with the values reported by Neese et al.[20] for the SOMO of a Cu_A complex, also reflecting the characteristic Cu-*d* and S-*p* spin densities reported in the study of Solomon.[124] This suggests once more the reduced species **1** as a possible starting point for the development of a Cu_A-like system.

For the HOMO of the neutral charged system, however, we determine a much larger delocalization over the entire molecule. For both derivatives, **1** and **2**, only 22% arise from Cu, and 35% (33% for **2**) from the bridging S atoms. Hence, the ratio between the Cu and the S contribution to the HOMO also corresponds to the distribution of the magnetization density shown in Figure 6. This suggests that the HOMOs ϕ_α^H and ϕ_β^H of the two spin channels can serve as a pair of *magnetic* orbitals.[112] Indeed, by restricting the analysis of the expectation value $\langle S^2 \rangle_{BS}$ in eq. (6) to this pair of orbitals exclusively, we reproduce within $\pm$0.05 the values obtained using the full set of orbitals (Table 3). In Figure 11, it is shown that the corresponding overlap stems predominantly from the Cu_2S_2 diamond core. A surprisingly large overlap is also found at the Cl and Br ligands. This overlap is slightly larger for the Br derivative **2** than for **1**. The largest overlap, however, is found at the S atoms bridging the two Cu nuclei, conclusively confirming the super-exchange character of the antiferromagnetic coupling within the Cu_2S_2 diamond core.

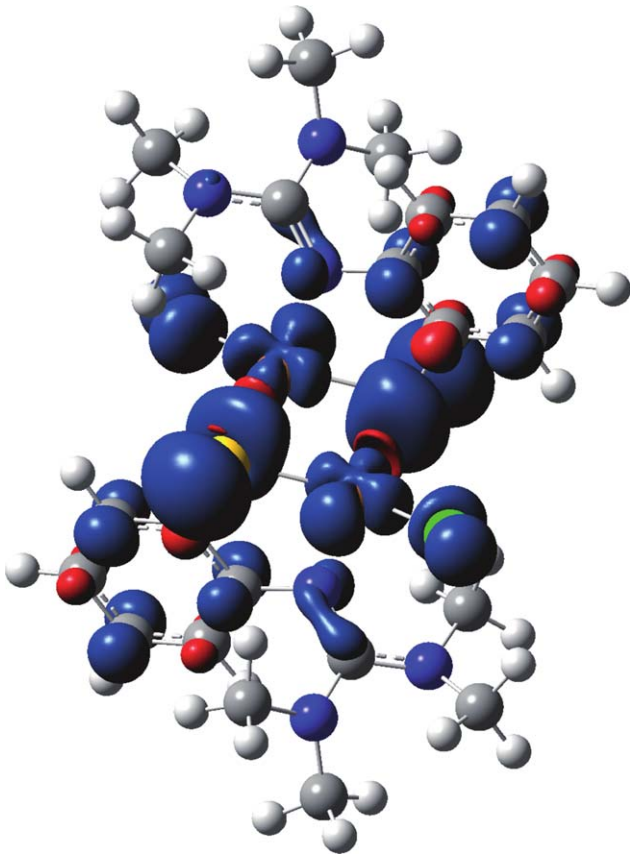

Figure 8. Calculated magnetization density of the mixed valence species in **1** in C_i symmetry within TPSSh+D3BJ/cc-pVDZ. The magnetization density is predominantly given by the SOMO. [Color figure can be viewed in the online issue, which is available at wileyonlinelibrary.com.]

Conclusions

In conclusion, DFT calculations for $Cu_2(NGuaS)_2Cl_2$ and its bromo derivative, both in gas-phase and in molecular crystals, are performed. The structural and electronic properties of the neutral species depend sensitively on the choice of the XC

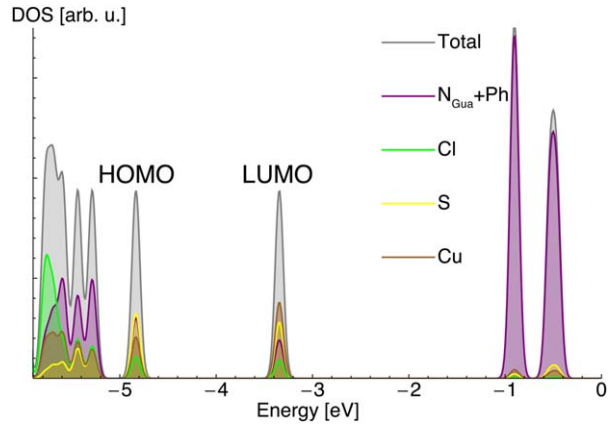

Figure 9. Density of states (DOS) for the BS state of **1**, here calculated with TPSSh+D3BJ/cc-pVDZ, broken down into total, Cu, S, Cl, and N(Gua) contributions. The energy (eV) is given with respect to the vacuum level; HOMO and LUMO levels are also indicated. [Color figure can be viewed in the online issue, which is available at wileyonlinelibrary.com.]

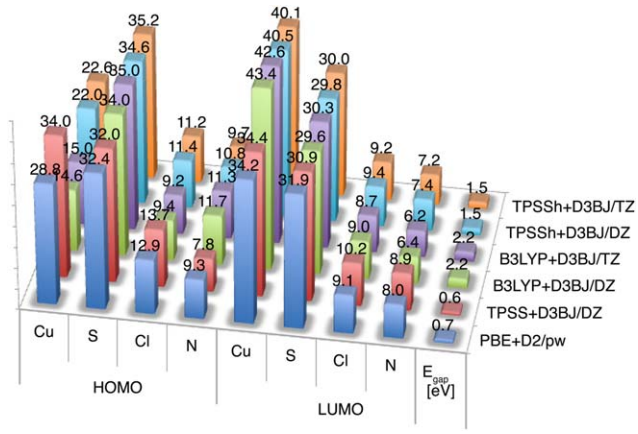

Figure 10. Calculated atomic contributions to the HOMO and LUMO as well as the band gap compared for several functionals and basis sets, determined for the BS state of **1** in the gas phase. [Color figure can be viewed in the online issue, which is available at wileyonlinelibrary.com.]

functional and provide a major challenge for DFT: whereas (i) the multideterminant character of the wave function of the neutral complexes is covered by the BS approach, (ii) meta-GGAs, that is hybrid functionals with an explicit dependence on the kinetic energy of the individual orbitals, are required to obtain the correct atomic structures. In combination with the BS approach, the TPSSh functional provides particularly meaningful results for the neutral Cu(II) thiolate complexes, reducing the Cu—Cu distance toward the experimentally observed value of 2.7 Å. The molecular ground state can be characterized by an antiferromagnetic electronic structure with nonvanishing absolute magnetic moment of about $m_{abs} \approx 1.4-1.9\,\mu_B$. Hence, the coupling is driven by super exchange interaction via the sulfur atoms within the Cu_2S_2 core. The coupling constants are calculated with the help of two different spin decontamination schemes ("NI" and "XD"). Within the second scheme, we present an interpretation in terms of the total spin S and m_{abs} exclusively. Both quantities are directly accessible in DFT, allowing an *ad hoc* spin decontamination. Afterward, the total energy curve of the multideterminant singlet state is reconstructed. For both schemes, the multideterminant ground state singlet energy is found to be 1.48 kcal/mol (64 meV) below the BS energy. SOC effects are of minor importance; their influence on the total energies as well as the intramolecular coupling constants is nearly negligible. Owing to the folded structure of **1**, puckered at the S atoms, the overlap of the HOMOs of the spin-up and -down channel is nearly maximized, offering a quite sensitive and extremely efficient antiferromagnetic coupling pathway. Consequently, the exchange coupling constants depend very sensitively on the structural environment. Molecule–molecule interactions in the crystalline structure are crucial to reproduce the experimental value for the bromo derivative **2**.

For the negative charge state of the complex, a mixed-valent $[Cu^{1.5+}\ldots Cu^{1.5+}]$ electronic structure with a rather small Cu—Cu distance of 2.6 Å is predicted, closer to the value of the Cu_A site of cytochrome *c* oxidase. Hence, the negative

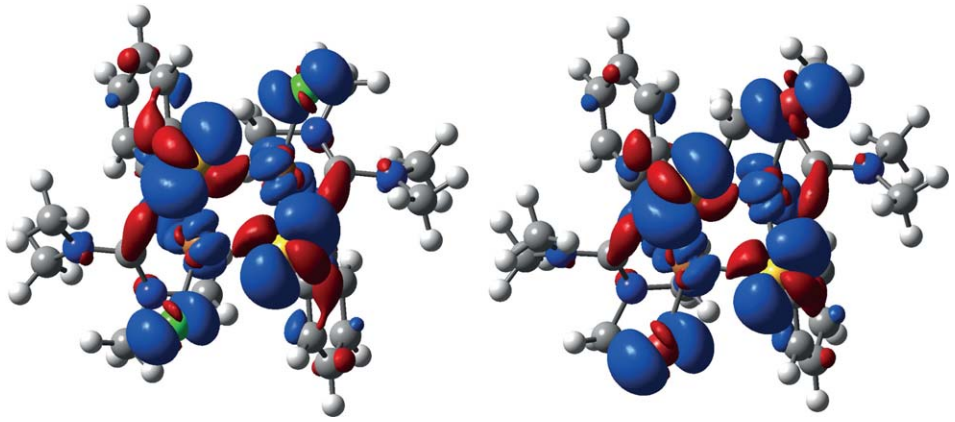

Figure 11. Overlap $\phi_\alpha^H(\vec{r})\phi_\beta^H(\vec{r})$ of the HOMO orbitals of the two spin channels α and β calculated on the TPSSh/cc-pVDZ level of theory for **1** (*left*) and the bromo derivative **2** (*right*). [Color figure can be viewed in the online issue, which is available at wileyonlinelibrary.com.]

complex $[Cu^{II}_2(NGuaS)_2Cl_2]^-$ provides a promising candidate to show Cu_A functionality. Further experimental study is necessary to prepare the reduced $Cu^{II}_2(NGuaS)_2Cl_2$ species and to analyze its microscopic and electronic structure, for example, by X-ray and EPR spectroscopy.

Acknowledgment

The Paderborn Center for Parallel Computing PC² is gratefully acknowledged.

Keywords: DFT · broken symmetry · CuA site · dicopper thiolate · super exchange

How to cite this article: M. Witte, U. Gerstmann, A. Neuba, G. Henkel, W. G. Schmidt. *J. Comput. Chem.* **2016**, *37*, 1005–1018. DOI: 10.1002/jcc.24289

[1] S. Iwata, C. Ostermeier, B. Ludwig, H. Michel, *Nature* **1995**, *376*, 660.
[2] M. Wilmanns, P. Lappalainen, M. Kelly, E. Sauer-Eriksson, M. Saraste, *Proc. Natl. Acad. Sci. USA* **1995**, *92*, 11955.
[3] T. Tsukihara, H. Aoyama, E. Yamashita, T. Tomizaki, H. Yamaguchi, K. Shinzawa-Itoh, R. Nakashima, R. Yaono, S. Yoshikawa, *Science* **1995**, *269*, 1069.
[4] G. Henkel, A. Müller, S. Weissgräber, G. Buse, T. Soulimane, G. C. M. Steffens, H. F. Nolting, *Angew. Chem. Int. Ed. Engl.* **1995**, *34*, 1488.
[5] N. J. Blackburn, S. De Vries, M. E. Barr, R. P. Houser, W. B. Tolman, D. Sanders, J. A. Fee, *J. Am. Chem. Soc.* **1997**, *119*, 6135.
[6] K. Brown, M. Tegoni, M. Prudencio, A. S. Pereira, S. Besson, J. J. Moura, I. Moura, C. Cambillau, *Nat. Struct. Biol.* **2000**, *7*, 1991.
[7] K. Paraskevopoulos, S. V. Antonyuk, R. G. Sawers, R. R. Eady, S. S. Hasnain, *J. Mol. Biol.* **2006**, *362*, 55.
[8] B. M. Hoffman, J. E. Roberts, M. Swanson, S. H. Speck, E. Margoliash, *Proc. Natl. Acad. Sci. USA* **1980**, *77*, 1452.
[9] T. H. Stevens, C. T. Martin, H. Wang, G. W. Brudvig, C. P. Scholes, S. I. Chan, *J. Biol. Chem.* **1982**, *257*, 12106.
[10] M. Hay, J. H. Richards, Y. Lu, *Proc. Natl. Acad. Sci. USA* **1996**, *93*, 461.
[11] P. Lappalainen, R. Aasa, B. G. Malmström, M. Saraste, *J. Biol. Chem.* **1993**, *268*, 26416.
[12] J. A. Farrar, F. Neese, P. Lappalainen, P. M. H. Kroneck, M. Saraste, W. G. Zumft, A. J. Thomson, D. Karlsruhe, *J. Am. Chem. Soc.* **1996**, *118*, 11501.
[13] C. R. Andrew, R. Fraczkiewicz, R. S. Czernuszewicz, P. Lappalainen, M. Saraste, J. Sanders-Loehr, *J. Am. Chem. Soc.* **1996**, *118*, 10436.
[14] T. Tsukihara, H. Aoyama, E. Yamashita, T. Tomizaki, H. Yamaguchi, K. Shinzawa-Itoh, R. Nakashima, R. Yaono, S. Yoshikawa, *Science* **1996**, *272*, 1136.
[15] C. T. Martin, C. P. Scholes, S. I. Chan, *J. Biol. Chem.* **1988**, *263*, 8420.
[16] C. Fan, J. F. Bank, R. G. Dorr, C. P. Scholes, *J. Biol. Chem.* **1988**, *263*, 3588.
[17] A. P. Hansen, R. D. Britt, M. P. Klein, C. J. Bender, G. T. Babcock, *Biochemistry* **1993**, *32*, 13718.
[18] R. Gurbiel, Y. Fann, K. K. Surerus, M. M. Werst, S. M. Musser, P. E. Doan, S. I. Chan, J. A. Fee, M. Brian Hoffman, *Contribution, J. Am. Chem. Soc.* **1993**, *115*, 10888.
[19] F. Neese, R. Kappl, J. Hüttermann, W. G. Zumft, P. M. H. Kroneck, *J. Biol. Inorg. Chem.* **1998**, *3*, 53.
[20] F. Neese, W. G. Zumft, W. E. Antholine, P. M. H. Kroneck, *J. Am. Chem. Soc.* **1996**, *118*, 8692.
[21] P. M. Colman, H. C. Freeman, J. M. Guss, M. Murata, V. A. Norris, J. A. M. Ramshaw, M. P. Venkatappa, *Nature* **1978**, *272*, 319.
[22] K. W. Penfield, A. Gewirth, E. I. Solomon, *J. Am. Chem. Soc.* **1985**, *107*, 4519.
[23] S. E. Shadle, J. E. Pennerhahn, H. J. Schugar, B. Hedman, K. O. Hodgson, E. I. Solomon, *J. Am. Chem. Soc.* **1993**, *115*, 767.
[24] D. W. Randall, S. D. George, B. Hedman, K. O. Hodgson, K. Fujisawa, E. I. Solomon, *J. Am. Chem. Soc.* **2000**, *122*, 11620.
[25] E. I. Solomon, R. K. Szilagyi, S. D. George, L. Basumallick, *Chem. Rev.* **2004**, *104*, 419.
[26] E. I. Solomon, B. Hedman, K. O. Hodgson, A. Dey, R. K. Szilagyi, *Coord. Chem. Rev.* **2005**, *249*, 97.
[27] E. I. Solomon, *Inorg. Chem.* **2006**, *45*, 8012.
[28] M. Hay, M. Ang, D. Gamelin, E. Solomon, W. Antholine, M. Ralle, N. Blackburn, P. Massey, X. Wang, A. Kwon, Y. Lu. *Inorg. Chem.* **1998**, *37*, 191.
[29] Y. Ueno, Y. Tachi, S. Itoh, *J. Am. Chem. Soc.* **2002**, *124*, 12428.
[30] A. I. Uraev, I. S. Vasilchenko, V. N. Ikorskii, T. Shestakova, A. S. Burlov, K. Lyssenko, V. G. Vlasenko, T. Kuzmenko, L. N. Divaeva, I. V. Pirog, G. S. Borodkin, I. E. Uflyand, M. Y. Antipin, V. I. Ovcharenko, A. D. Garnovskii, V. I. Minkin. *Mendeleev Commun.* **2005**, *15*, 133.
[31] R. P. Houser, J. Halfen, V. G. Young, N. J. Blackbum, W. B. Tolman, *J. Am. Chem. Soc.* **1995**, *117*, 10745.
[32] S. Itoh, M. Nagagawa, S. Fukuzumi, *J. Am. Chem. Soc.* **2001**, *123*, 4087.
[33] W. Rammal, C. Belle, C. Béguin, C. Duboc, C. Philouze, J. L. Pierre, L. Le Pape, S. Bertaina, E. Saint-Aman, S. Torelli, *Inorg. Chem.* **2006**, *45*, 10355.
[34] N. Roy, S. Sproules, E. Bothe, T. Weyhermuller, K. Wieghardt, *Eur. J. Inorg. Chem.* **2009**, *2009*, 2655.
[35] N. D. J. Branscombe, A. J. Blake, A. Marin-Becerra, W. S. Li, S. Parsons, L. Ruiz-Ramirez, M. Schroeder, *Chem. Commun.* **1996**, *1*, 2573.
[36] S. Torelli, M. Orio, J. Pécaut, H. Jamet, L. L. Pape, S. Ménage, *Angew. Chem. Int. Ed.* **2010**, *49*, 8249.

[37] S. Torelli, M. Orio, J. Pécaut, H. Jamet, L. L. Pape, S. Ménage, *Angew. Chem. Int. Ed.* **2010**, *122*, 8425.
[38] R. T. Stibrany, R. Fikar, M. Brader, M. N. Potenza, J. A. Potenza, H. J. Schugar, *Inorg. Chem.* **2002**, *41*, 7.
[39] A. Neuba, U. Flörke, W. Meyer-Klaucke, M. Salomone-Stagni, E. Bill, E. Bothe, P. Höfer, G. Henkel, *Angew. Chem.* **2011**, *123*, 4596.
[40] A. Neuba, U. Flörke, W. Meyer-Klaucke, M. Salomone-Stagni, E. Bill, E. Bothe, P. Höfer, G. Henkel, *Angew. Chem. Int. Ed.* **2011**, *50*, 4503.
[41] R. P. Houser, V. G. Young, W. B. Tolman, *J. Am. Chem. Soc.* **1996**, *118*, 2101.
[42] E. I. Solomon, X. Xie, A. Dey, *Chem. Soc. Rev.* **2008**, *37*, 623.
[43] M. Gennari, J. Pécaut, S. DeBeer, F. Neese, M. N. Collomb, C. Duboc, *Angew. Chem. Int. Ed.* **2011**, *50*, 5662.
[44] M. R. Jensen, F. Hansen, J. J. Led, *J. Am. Chem. Soc.* **2002**, *124*, 4093.
[45] A. Neuba, R. Haase, W. Meyer-Klaucke, U. Flörke, G. Henkel, *Angew. Chem. Int. Ed.* **2012**, *51*, 1714.
[46] F. Neese, *Coord. Chem. Rev.* **2009**, *253*, 526.
[47] C. Blanchet-Boiteux, J. Mouesca, *J. Phys. Chem. A* **2000**, *104*, 2091.
[48] B. F. Gherman, C. J. Cramer, *Coord. Chem. Rev.* **2009**, *253*, 723.
[49] P. W. Anderson, *Phys. Rev.* **1950**, *79*, 350.
[50] L. Noodleman, J. G. Norman, *J. Chem. Phys.* **1979**, *70*, 4903.
[51] L. Noodleman, *J. Chem. Phys.* **1981**, *74*, 5737.
[52] L. Noodleman, E. J. Baerends, *J. Am. Chem. Soc.* **1984**, *106*, 2316.
[53] L. Noodleman, D. Case, *Adv. Inorg. Chem* **1992**, *38*, 423.
[54] J. P. Malrieu, G. Trinquier, *J. Phys. Chem. A* **2012**, *116*, 8226.
[55] M. J. Frisch, G. W. Trucks, H. B. Schlegel, G. E. Scuseria, M. A. Robb, J. R. Cheeseman, G. Scalmani, V. Barone, B. Mennucci, G. A. Petersson, H. Nakatsuji, M. Caricato, X. Li, H. P. Hratchian, A. F. Izmaylov, J. Bloino, G. Zheng, J. L. Sonnenberg, M. Hada, M. Ehara, K. Toyota, R. Fukuda, J. Hasegawa, M. Ishida, T. Nakajima, Y. Honda, O. Kitao, H. Nakai, T. Vreven, J. A. Montgomery, Jr., J. E. Peralta, F. Ogliaro, M. Bearpark, J. J. Heyd, E. Brothers, K. N. Kudin, V. N. Staroverov, R. Kobayashi, J. Normand, K. Raghavachari, A. Rendell, J. C. Burant, S. S. Iyengar, J. Tomasi, M. Cossi, N. Rega, J. M. Millam, M. Klene, J. E. Knox, J. B. Cross, V. Bakken, C. Adamo, J. Jaramillo, R. Gomperts, R. E. Stratmann, O. Yazyev, A. J. Austin, R. Cammi, C. Pomelli, J. W. Ochterski, R. L. Martin, K. Morokuma, V. G. Zakrzewski, G. A. Voth, P. Salvador, J. J. Dannenberg, S. Dapprich, A. D. Daniels, Ö. Farkas, J. B. Foresman, J. V. Ortiz, J. Cioslowski, D. J. Fox, *Gaussian09*, **2009**.
[56] P. Giannozzi, S. Baroni, N. Bonini, M. Calandra, R. Car, C. Cavazzoni, D. Ceresoli, G. L. Chiarotti, M. Cococcioni, I. Dabo, A. D. Corso, S. de Gironcoli, S. Fabris, G. Fratesi, R. Gebauer, U. Gerstmann, C. Gougoussis, A. Kokalj, M. Lazzeri, L. Martin-Samos, N. Marzari, F. Mauri, R. Mazzarello, S. Paolini, A. Pasquarello, L. Paulatto, C. Sbraccia, S. Scandolo, G. Sclauzero, A. P. Seitsonen, A. Smogunov, P. Umari, R. M. Wentzcovitch, *J. Phys. Condens. Matter* **2009**, *21*, 395502.
[57] T. H. Dunning, *J. Chem. Phys.* **1989**, *90*, 1007.
[58] N. B. Balabanov, K. A. Peterson, *J. Chem. Phys.* **2005**, *123*, 064107.
[59] D. E. Woon, T. H. Dunning, *J. Chem. Phys.* **1993**, *98*, 1358.
[60] J. P. Perdew, A. Ruzsinszky, J. Tao, V. N. Staroverov, G. E. Scuseria, *J. Chem. Phys.* **2005**, *123*, 062201.
[61] D. M. Ceperley, B. J. Alder, *Phys. Rev. Lett.* **1980**, *45*, 566.
[62] J. P. Perdew, A. Zunger, *Phys. Rev. B* **1981**, *23*, 5048.
[63] J. P. Perdew, Y. Wang, *Phy. Rev. B* **1992**, *45*, 13244.
[64] J. P. Perdew, K. Burke, M. Ernzerhof, *Phys. Rev. Lett.* **1996**, *77*, 3865.
[65] C. Lee, W. Yang, R. G. Parr, *Phys. Rev. B* **1988**, *37*, 785.
[66] A. D. Becke, *J. Chem. Phys.* **1993**, *98*, 5648.
[67] A. D. Becke, *J. Comput. Chem.* **1999**, *20*, 63.
[68] J. Tao, J. Perdew, V. Staroverov, G. Scuseria, *Phys. Rev. Lett.* **2003**, *91*, 146401.
[69] V. N. Staroverov, G. E. Scuseria, J. Tao, J. P. Perdew, *J. Chem. Phys.* **2004**, *121*, 11507.
[70] V. N. Staroverov, G. E. Scuseria, J. Tao, J. P. Perdew, *J. Chem. Phys.* **2003**, *119*, 12129.
[71] F. Neese, W. Ames, G. Christian, M. Kampa, D. G. Liakos, D. A. Pantazis, M. Roemelt, P. Surawatanawong, Y. Shengfa, In Advances in Inorganic Chemistry, Vol. *62*; R. van Eldik, J. Harvey, Eds.; Academic Press, Cambridge, Massachusetts, **2010**; pp. 301–349.
[72] M. Rohlfing, T. Bredow, *Phys. Rev. Lett.* **2008**, *101*, 266106.
[73] M. Dion, H. Rydberg, E. Schröder, D. C. Langreth, B. I. Lundqvist, *Phys. Rev. Lett.* **2004**, *92*, 246401.
[74] M. Dion, H. Rydberg, E. Schröder, D. Langreth, B. Lundqvist, *Phys. Rev. Lett.* **2005**, *95*, 109902.
[75] D. C. Langreth, M. Dion, H. Rydberg, E. Schröder, P. Hyldgaard, B. I. Lundqvist, *Int. J. Quantum Chem.* **2005**, *101*, 599.
[76] F. Ortmann, W. G. Schmidt, F. Bechstedt, *Phys. Rev. Lett.* **2005**, *95*, 186101.
[77] F. Ortmann, F. Bechstedt, W. G. Schmidt, *Phys. Rev. B* **2006**, *73*, 205101.
[78] A. Tkatchenko, M. Scheffler, *Phys. Rev. Lett.* **2009**, *102*, 073005.
[79] C. Thierfelder, M. Witte, S. Blankenburg, E. Rauls, W. G. Schmidt, *Surf. Sci.* **2011**, *605*, 746.
[80] E. R. Mcnellis, J. Meyer, K. Reuter, *Phys. Rev. B* **2009**, *80*, 205414.
[81] S. Grimme, *J. Comput. Chem.* **2006**, *27*, 1787.
[82] S. Grimme, S. Ehrlich, L. Goerigk, *J. Comput. Chem.* **2011**, *32*, 1456.
[83] S. Luo, I. Rivalta, V. Batista, D. G. Truhlar, *J. Phys. Chem. Lett.* **2011**,
[84] L. L. Foldy, S. A. Wouthuysen, *Phys. Rev.* **1950**, *78*, 29.
[85] E. van Lenthe, E. J. Baerends, J. G. Snijders, *J. Chem. Phys.* **1993**, *99*, 4597.
[86] C. Klein, N. J. Vollmers, U. Gerstmann, P. Zahl, D. Lükermann, G. Jnawali, H. Pfnür, C. Tegenkamp, P. Sutter, W. G. Schmidt, M. Horn-von Hoegen, *Phys. Rev. B* **2015**, *91*, 195441.
[87] U. Gerstmann, N. J. Vollmers, A. Lücke, M. Babilon, W. G. Schmidt, *Phys. Rev. B* **2014**, *89*, 165431
[88] S. I. Gorelsky, X. Xie, Y. Chen, J. A. Fee, E. I. Solomon, *J. Am. Chem. Soc.* **2006**, *128*, 16452.
[89] M. H. M. Olsson, U. Ryde, *J. Am. Chem. Soc.* **2001**, *123*, 7866.
[90] D. G. Liakos, F. Neese, *J. Chem. Theory Comput.* **2011**, *7*, 1511.
[91] M. Rohrmüller, S. Herres-Pawlis, M. Witte, W. G. Schmidt, *J. Comput. Chem.* **2013**, *34*, 1035.
[92] J. Halfen, S. Mahapatra, E. C. Wilkinson, S. Kaderli, V. G. Young, L. Que, A. D. Zuberbühler, W. B. Tolman, *Science* **1996**, *271*, 1397.
[93] A. G. Blackman, W. B. Tolman, In Structure and Bonding, Vol. *97*; B. Meunier, Ed.; Springer: Berlin, Heidelberg, **2000**; pp. 179–211.
[94] B. T. Op't Holt, M. A. Vance, L. M. Mirica, D. E. Heppner, T. D. P. Stack, E. I. Solomon, *J. Am. Chem. Soc.* **2009**, *131*, 6421.
[95] V. Barone, M. Casarin, D. Forrer, M. Pavone, M. Sambi, A. Vittadini, *J. Comput. Chem.* **2009**, *30*, 934.
[96] Y. Takano, Y. Shigeta, K. Koizumi, H. Nakamura, *Int. J. Quantum Chem* **2012**, *112*, 208.
[97] M. Reiher, *Inorg. Chem.* **2002**, *41*, 6928.
[98] H. Paulsen, L. Duelund, H. Winkler, H. Toftlund, A. X. Trautwein, *Inorg. Chem.* **2001**, *40*, 2201.
[99] R. J. Deeth, N. Fey, *J. Comput. Chem.* **2004**, *25*, 1840.
[100] M. Swart, A. Groenhof, A. Ehlers, K. Lammertsma, *J. Phys. Chem. A* **2004**, *108*, 5479.
[101] E. Ruiz, A. Rodríguez-Fortea, J. Cano, S. Alvarez, P. Alemany, *J. Comput. Chem.* **2003**, *24*, 980.
[102] S. Herres-Pawlis, P. Verma, R. Haase, P. Kang, C. T. Lyons, E. C. Wasinger, U. Flörke, G. Henkel, T. D. P. Stack, *J. Am. Chem. Soc.* **2009**, *131*, 1154.
[103] C. J. Calzado, J. Cabrero, J. P. Malrieu, R. Caballol, *J. Chem. Phys.* **2002**, *116*, 3985.
[104] M. Zbiri, S. Saha, C. Adhikary, S. Chaudhuri, C. Daul, S. Koner, *Inorg. Chim. Acta* **2006**, *359*, 1193.
[105] O. Kahn, Molecular Magnetism, 1st ed.; Wiley-VCH: Weinheim, **1993**.
[106] M. Nishino, S. Yamanaka, Y. Yoshioka, K. Yamaguchi, *J. Phys. Chem. A* **1997**, *101*, 705.
[107] A. Bencini, F. Totti, C. Daul, K. Doclo, P. Fantucci, V. Barone, *Inorg. Chem.* **1997**, *36*, 5022.
[108] E. Ruiz, J. Cano, S. Alvarez, P. Alemany, *J. Comput. Chem.* **1999**, *20*, 1391.
[109] P. O. Löwdin, *Phys. Rev.* **1955**, *97*, 1490.
[110] A. J. Cohen, D. J. Tozer, N. C. Handy, *J. Chem. Phys.* **2007**, *126*, 214104.
[111] J. Gräfenstein, D. Cremer, *Mol. Phys.* **2001**, *99*, 981.
[112] F. Neese, *J. Phys. Chem. Solids* **2004**, *65*, 781.
[113] M. Ali, S. Datta, *J. Phys. Chem. A* **2006**, *110*, 2776.
[114] M. Ali, S. Datta, *J. Mol. Struct. Theochem.* **2009**, *775*, 19.
[115] J. Wang, A. D. Becke, V. H. Smith, *J. Chem. Phys.* **1995**, *102*, 3477.
[116] Y. Kitagawa, T. Saito, Y. Nakanishi, Y. Kataoka, T. Matsui, T. Kawakami, M. Okumura, K. Yamaguchi, *J. Phys. Chem. A* **2009**, *113*, 15041.
[117] N. Ferré, N. Guihéry, J. P. Malrieu, *Phys. Chem. Chem. Phys.* **2015**, *17*, 14375.
[118] K. Yamaguchi, F. Jensen, A. Dorigo, K. Houk, *Chem. Phys. Lett.* **1988**, *149*, 537.
[119] J. V. Burda, M. Pavelka, M. Šimánek, *J. Mol. Struct. Theochem.* **2004**, *683*, 183.

[120] T. Shi, S. He, X. Wang, Y. Wang, Z. Tang, Z. Wen, *J. Mol. Struct. Theochem.* **2005**, *732*, 201.
[121] H. L. Hermann, G. Boche, P. Schwerdtfeger, *Chem. Eur. J.* **2001**, *7*, 5333.
[122] M. G. Banks, R. K. Kremer, C. Hoch, A. Simon, B. Ouladdiaf, J. M. Broto, H. Rakoto, C. Lee, M. H. Whangbo, *Phys. Rev. B Condens. Matter* **2009**, *80*, 1.
[123] S. Seki, T. Kurumaji, S. Ishiwata, H. Matsui, H. Murakawa, Y. Tokunaga, Y. Kaneko, T. Hasegawa, Y. Tokura, *Phys. Rev. B Condens. Matter* **2010**, *82*, 1.
[124] S. DeBeer George, M. Metz, R. K. Szilagyi, H. Wang, S. P. Cramer, Y. Lu, W. B. Tolman, B. Hedman, K. O. Hodgson, E. I. Solomon, *J. Am. Chem. Soc.* **2001**, *123*, 5757.

Received: 15 July 2015
Revised: 30 November 2015
Accepted: 2 December 2015
Published online on 24 January 2016